Effect of thickness and frequency of applied field on the switching dynamics of multiferroic bismuth ferrite thin films

Chhatra R. Joshi,[1] Mahendra Acharya,[2] Gary J. Mankey,[1] and Arunava Gupta[2,3,*]

[1]*Department of Physics and Astronomy, The University of Alabama, Tuscaloosa, Alabama 35487, USA*

[2]*Department of Chemistry and Biochemistry, The University of Alabama, Tuscaloosa, Alabama 35487, USA*

[3]*Department of Chemical and Biological Engineering, The University of Alabama, Tuscaloosa, Alabama 35487, USA*

(Received 7 March 2022; accepted 28 April 2022; published 19 May 2022)

Epitaxial films of multiferroic $BiFeO_3$ (BFO) with different thicknesses are grown on $SrRuO_3$ buffered $SrTiO_3$ (001) substrates using the pulsed laser deposition technique. The room-temperature polarization-voltage (P-V) hysteresis loop, leakage current and average domain size of films with varying thicknesses have been investigated. The frequency dependence of the coercive voltage and variation of the coercive voltage as a function of film thickness are ascertained to examine the validity of the Ishibashi-Orihara model and the semi-empirical Kay-Dunn scaling relationship, respectively. The results demonstrate that at room temperature the BFO films indeed follow the Ishibashi-Orihara (I-O) model and Kay-Dunn scaling law. The dimensionality of the domains acquired by piezoresponse force microscopy imaging further validates that found from the I-O model scaling exponent and is consistent with Kittel's law regarding dependence of domain width on film thickness. These combined results elucidate the fundamental properties that govern the switching kinetics of BFO and are relevant for BFO-based multiferroic materials in next generation logic and memory devices operating over a wide range of frequencies.

DOI: 10.1103/PhysRevMaterials.6.054409

I. INTRODUCTION

Materials in which ferroelectricity and (anti)ferromagnetism coexist are referred to as multiferroic (MF) materials [1–4]. $BiFeO_3$ (BFO), perhaps the most extensively studied room temperature (RT) multiferroic material [5–7], exhibits both ferroelectricity as well as antiferromagnetic order with a small canted magnetic moment and with relatively higher transition temperatures ($T_N \sim 640$ K and $T_C \sim 1100$ K) [5,8]. Since the initial experimental demonstration of coupling between antiferromagnetic and ferroelectric domains in BFO there has been much interest in the possibility of controlling magnetic properties by application of an electric field [8,9]. Indeed, BFO exhibits promising room-temperature magnetoelectric properties and is being considered for low energy nonvolatile magnetoelectric spin orbit (MESO) logic devices [10]. Considering the potential application of BFO in next-generation devices [7,11,12], we have investigated its switching dynamics over a wide range of film thickness and frequency of applied field.

The switching dynamics of ferroelectric (FE) and/or ferromagnetic (FM) materials can be probed either in the time domain (for different frequencies of the applied electric and/or magnetic field) or as a function of film thickness. Understanding these properties are critical for potential applications in ultrafast switching devices such as FE/FM random access memory and sensors [13,14]. Since the coercive field is a function of film thickness and frequency of the applied field, it is important to understand how the switching mechanism depends on these parameters. Devices are normally designed to operate over a wide range of frequencies; thus, knowledge of the frequency dependence of coercive field is crucial for optimizing their response. Experiments to determine the dynamic hysteresis loops are generally performed by applying a sinusoidal or triangular external field with varying amplitude or frequency. There have been several studies of the amplitude and frequency dependence of the FM hysteresis loops, some dating back one hundred years or more [15,16]. The power law for frequency-dependent coercive field is followed by FM [13,17] as well as FE materials [18]. There have been only a few recent theoretical and experimental papers to systematically study the frequency-dependent ferroelectric properties such as the coercive voltage and polarization [14,18–26]. For ferromagnets and ferroelectrics, the coercivity increases with frequency of applied field due to analogous physical phenomena. Correlating known FM domain properties with that of FE materials enables direct comparison to relatively new and less explored avenues of FE materials.

Here we present a systematic study of the room temperature coercive voltage for different thickness BFO films over a wide-frequency range. The kinetics of switching is governed primarily by domain wall motion. The domain wall velocity depends on the frequency of applied field since their movement is impeded by viscous forces as they move in the FE medium. With application of higher frequency (shorter pulses) the domain walls move faster, and as a result the viscosity increases, requiring a higher switching voltage [27]. A phenomenological model describing the frequency dependence of coercive voltage was developed by Ishibashi and Orihara (I-O model) based on the Avrami model for kinetics of crystalline growth [19]. This model assumes that the velocity of the

*Corresponding author: arunava.gupta@ua.edu

domain wall is a function of field strength. In the I-O model, the mathematical relationship between coercive voltage (V_c) and frequency (f) is given by,

$$V_c \propto f^{\beta} \tag{1}$$

with

$$\beta = d/\alpha, \tag{2}$$

where "d" is the effective dimension of switching domains in the ferroelectric material and α has a value of approximately 6 for sinusoidal and triangular wave signals. The value of "d" is 1 for domains with straight planar walls parallel to each other [18]. As the domain walls become curved and develop a labyrinth structure the value of d decreases following a fractal dimension [28].

The film thickness also has a significant influence on the coercive field, domain shape and sizes, and leakage current of FE thin films. The coercive field determines the operating voltage for device operation, the polarization determines the charge storing capacity, while leakage current determines the device performance, with domain shape and size having control over all these properties. However, despite the need for better understanding of how the above-mentioned properties are influenced by the film thickness, there are only a few detailed reports on this topic [24,29–31]. It is recognized that the domain size scales with square root of film thickness for FM materials, which has also been extended to FE, ferroelastic as well as multiferroic materials [32,33]. The well-known scaling law of Landau, Lifshitz, and Kittel (LLK) states that the domain width (w) grows proportionally to the square root of film thickness (t), i.e. $w \propto t^{1/2}$.

The coercive field and associated switching of any FE materials involve complex processes that includes the nucleation, growth, and distribution of domains. The coercive voltage (V_c) is a kinetic parameter, and its dependence on thickness (t) has been phenomenologically explained by the semi-empirical Kay-Dunn scaling relationship (i.e., $V_c \propto t^{1/3}$) over a wide range of film thickness from a few nanometers to several micrometers [34]. We have used a FE tester to investigate the Kay-Dunn law for different thickness BFO films. However, high leakage current in relatively thinner films (less than ~70 nm) prevents acquisition of P-V loops. Thus, piezo-response force microscopy (PFM) technique has been used to study the scaling behavior for thinner films. It should be noted that ultrathin films (film thickness < 10 nm) do not follow the Kay-Dunn scaling behavior due to the depolarizing field, which acts opposite to the applied field. This deviation arises due to incomplete screening from the electric field of electrodes. The screening leads to a difference between the measured and true V_c in ultrathin films [35,36].

We have analyzed the domain wall dimension in BFO using a static method (i.e., PFM) and the findings have been validated using dynamic method (i.e., the I-O model). In addition, the thickness dependence of domain width and coercive voltage have been analyzed to examine the Kittel law and Kay-Dunn scaling law, respectively. The correlation between domain wall density and leakage current has also been demonstrated. These findings are useful to understand the switching dynamics in BFO and other related ferroic systems and thereby help design future generation logic and memory devices that need to be operated over a wide range of frequencies.

II. EXPERIMENTAL DETAILS

A bismuth ferrite ceramic target was prepared using a tartaric acid modified sol-gel method for use in film deposition. Bismuth nitrate [$Bi(NO_3)_3.5H_2O$], iron nitrate [$Fe(NO_3)_3.9H_2O$], and tartaric acid were taken with molar ratio 1.2:1:1 and mixed with 2-methoxy ethanol to produce a homogeneous mixture. 20% excess bismuth was used to compensate for Bi loss during target preparation and film fabrication. This mixture was stirred and heated at a temperature of 150 °C. The mixture in the form of a gel was then burnt at a temperature of 220 °C and transferred to a furnace and heated at 600 °C for 5 hours. A 1″ pellet die was then used to compact the powder and prepare the target. Subsequently, the target was heated at 700 °C for 10 hours for densification. The stoichiometry and surface morphology of the targets were studied using energy dispersive spectroscopy (EDS) and scanning electron microscopy (SEM, JEOL 7000). A commercially acquired high density target (Kojundo Chemical Laboratory Co. Ltd., Japan) was used for deposition of $SrRuO_3$ (SRO) films.

Epitaxial BFO thin films were fabricated on $SrTiO_3(001)$ (STO) and SRO buffered STO substrates using ceramic targets. Pulsed laser deposition (PLD) technique with 248 nm, KrF excimer laser (10 Hz/1.2 J cm^{-2} for BFO and 4 Hz/1.5 J cm^{-2} for SRO) was used for the deposition. Both SRO and BFO films were grown at 700 °C under a background oxygen pressure of 100 mTorr. The films were cooled down under the same oxygen pressure at 6 °C/min. The thickness of SRO bottom layer was maintained at 50 nm for all the heteroepitaxial structures.

The surface morphology of the films was studied with atomic force microscopy (AFM, Asylum Research MFP-3D) in tapping mode and scanning electron microscopy (SEM). Structural characterization was carried out using x-ray diffraction (Xpert Pro, Phillips) with Cu-K_α source. The film thickness and epitaxial quality were determined using x-ray reflectivity (XRR) and rocking curve measurements, respectively. The compositions of the films were determined by Rutherford backscattering (RBS) and energy dispersive x-ray spectroscopy (EDS). The thickness of a ~40 nm BFO//STO film was established using x-ray reflectivity (XRR) and was used to calibrate the number of laser pulses employed to grow thicker films. The thicknesses were reconfirmed using cross sectional SEM and RBS. Platinum (Pt) electrodes with thickness 60 nm and diameter 70 μm were deposited on top of the BFO films by DC magnetron sputtering using a shadow mask to realize capacitor structures (Pt//BFO//SRO). A ferroelectric tester (Radiant Tech., Precision Premier II) was utilized for leakage current measurements and ferroelectric characterization under ambient conditions. The AFM-based setup with Pt coated silicon tip having a force constant of 2.8 N/m was used for PFM measurements. The cantilever tip served as the top electrode whereas SRO served as the bottom electrode for the PFM measurements.

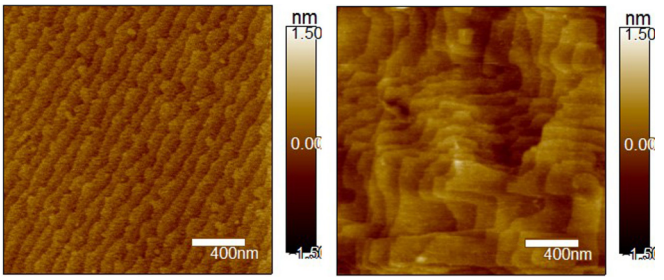

FIG. 1. AFM images of 50 nm SRO//STO showing RMS roughness of about 200 pm (left) and 110 nm BFO//SRO//STO with RMS roughness of about 300 pm (right).

III. RESULTS AND DISCUSSION

The ferroelectric properties critically depend on morphology of the bottom electrode as it constitutes the basis of the capacitor structure that has control over domain shape and growth pattern of the FE material. During growth process optimization, the roughness and surface qualities of SRO on STO and BFO on SRO buffered STO were analyzed using AFM imaging. Representative AFM images of optimized SRO grown on STO (left) and BFO grown on SRO buffered STO (right) are shown in Fig. 1. The AFM images show that SRO//STO film is of high quality having atomically flat surface with steps and terraces. Such a high-quality bottom electrode is desirable for ferro/piezo-electric measurements. The BFO heterostructure grown on top of SRO also exhibits atomically flat terraces with a root mean square (RMS) roughness of about 300 pm. For improved FE properties, as well as better film morphology, the deposition temperature, growth rate, quality of target material and substrate, and other process parameters play a crucial role.

Figure 2 shows θ-2θ scans near the (002) peak for three different thickness BFO films grown on SRO buffered STO. All the diffraction peaks are indexed and the out-of-plane lattice parameters calculated based on pseudo-cubic notation are consistent with previously reported values [37]. With

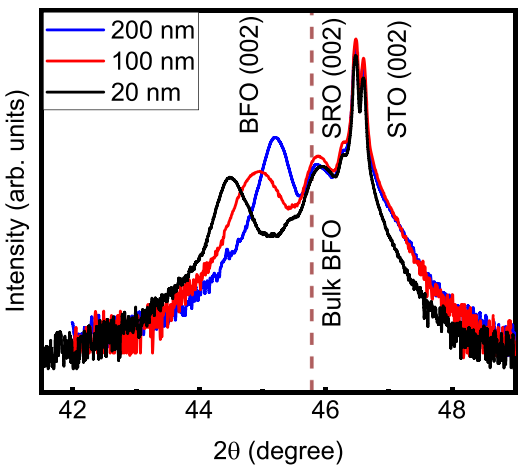

FIG. 2. θ-2θ XRD patterns for BFO films with different thicknesses grown on SRO//STO. Both BFO and SRO are crystallized as perovskite with a (00l) texture.

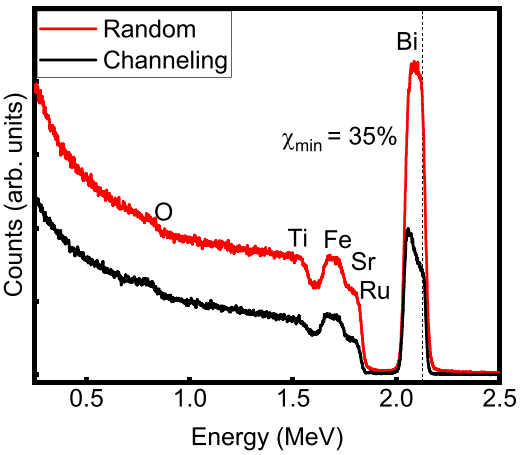

FIG. 3. Random (red) and aligned (black) RBS spectra for a 110 nm BFO//SRO//STO heterostructure.

increasing film thickness, the (00l) peaks shift towards higher angles indicating that the out-of-plane lattice parameter decreases. The out-of-plane lattice parameters for 20, 100, and 200 nm films are 4.07 Å, 4.03 Å, and 4.01 Å, respectively, and approaches the bulk value of 3.96 Å (2θ value corresponding to the bulk BFO is shown by a dashed line in Fig. 2) [5,37]. This is due to the progressively decreasing effect of compressive strain due to relaxation for relatively thicker films.

The composition analysis of BFO grown on SRO buffered STO has been carried out by Rutherford backscattering spectroscopy (RBS). A 2.3-MeV beam of He^{++} at normal incident angle is directed at the sample for the measurements. The energy distribution and yield of backscattered ions are determined at a scattering angle of 163° using a detector with energy resolution of 18 keV. The composition and thickness of the samples are obtained by fitting the experimental spectra using RBS analysis software SIMNRA [38]. A representative fit for a 110-nm BFO//SRO heterostructure is shown in Fig. 3. The peaks can be assigned to Bi, Fe, Ru, and Sr from the BFO and SRO films and to Sr and Ti for the substrate. The oxygen peak is not distinct due to its low atomic mass. The composition analysis shows that the ratio of Bi to Fe is nearly unity (Bi:Fe $= 0.98 \pm 0.02$) within the experimental error even though a 20% Bi rich target is used during the deposition. The thickness measurement is in agreement with the results obtained by using XRR and cross-sectional SEM. The RBS channeling χ_{min} data indicates that the films have comparable, if not better, crystalline quality compared to similar films reported in the literature [39]. Defects arise due to lattice mismatch with the substrate, oxygen and/or cation deficiency in BFO. BFO-based materials have higher χ_{min} in RBS channeling [39] as compared to other simpler oxides [40], therefore, the somewhat higher χ_{min} value in BFO is reasonable.

The hallmark of ferroelectricity is hysteresis of switchable polarization with the application of an applied voltage. P-V hysteresis loops are acquired to analyze the polarization switching behavior by applying a standard bipolar triangular waveform with different frequencies and amplitudes. A representative set of P-V loops over a wide-frequency range of

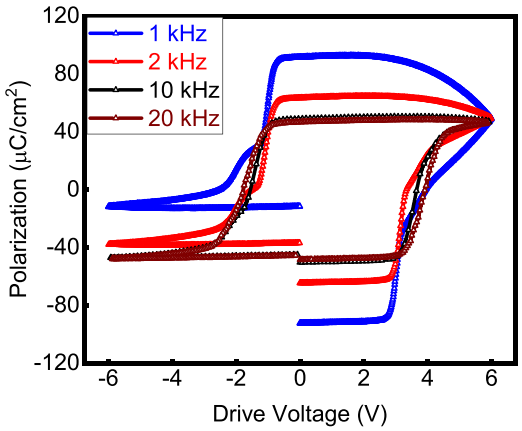

FIG. 4. P-V hysteresis loops for 110 nm BFO film with applied frequencies of 1−20 kHz.

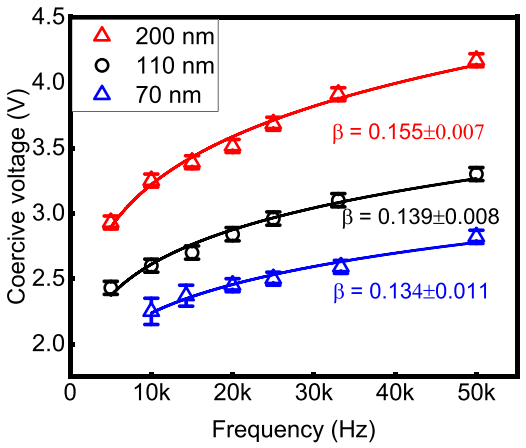

FIG. 6. Coercive voltage vs frequency plots for BFO films with different thicknesses. The solid lines represent power-law fit for the I-O model.

applied field is shown in Fig. 4. Open loops with abnormally high polarization values are observed at lower frequencies due to higher contribution of leakage current caused by application of voltage for relatively longer duration. Quantification of the coercive voltage and saturation polarization using open loops can be misleading, which has restricted the study of frequency dependence of V_c over a wider range of frequencies. To quantify these parameters, we have done a systematic analysis of P-V loops over a frequency range in which nearly closed loops are obtained.

The P-V loops for films under study are essentially closed in the frequency range of 5 to 50 kHz (signal with relatively shorter pulses). Smaller electrodes are required to obtain closed P-V loops at even higher frequencies as the switching time is proportional to the area of the capacitor [41]. Figure 5 shows that loops measured at high frequencies are not completely saturated and with somewhat lower remnant polarization as all the domains may not be switched since they cannot follow the change in the electric field. However, the P-V loops measured at lower frequencies are well saturated and exhibit intrinsic value of the remnant polarization. Consistent with the I-O model, at lower frequencies the loops

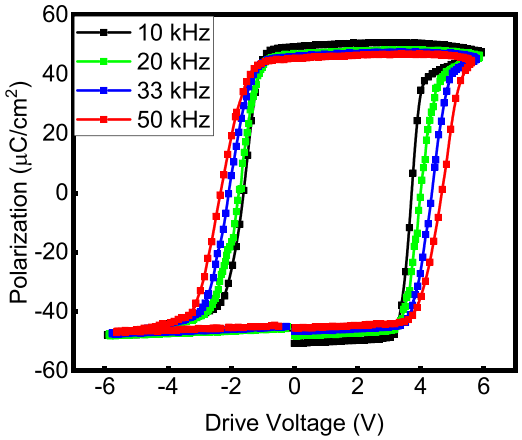

FIG. 5. P-V hysteresis loops for a 110-nm BFO film with applied frequencies of 10–50 kHz.

are narrower with lower V_c, whereas they broaden at higher frequencies [19,27].

The coercive voltage at each frequency is determined as the average using the mean value of V_c from both the polarities, $V_c = (|V_c^-| + |V_c^+|)/2$, where V_c^- and V_c^+ are negative and positive V_c's obtained from P-V hysteresis loop for 20 different capacitor structures measured in the same sample. The loops are not symmetric and the numerical values for V_c^- and V_c^+ are not equal due to the use of dissimilar top and bottom electrodes. To remove artifacts from unsaturated loops, the maximum amplitude of applied voltage is adjusted to be nearly twice V_c. To investigate the validity of the I-O model, the frequency dependence of coercive voltage for different thickness films are plotted as shown in Fig. 6. All exponents obtained from a power-law fit are in close agreement with the theoretically predicted value (∼0.16) from Eq. (1) and Eq. (2), corresponding to a "d" value near unity. This suggests that BFO has highly anisotropic uniaxial ferroelectric behavior where the nucleation is deterministic, indicating unidirectional domain wall motion over a significant portion of the switching time [27]. The apparent reduction of the β value for thinner films suggests that the domains may deviate from having straight planar walls to being somewhat curved with decreasing thickness. From energetic point of view, it is advantageous to have a "d" value of unity rather than higher value corresponding to bulk materials as the energy loss caused by hysteresis is directly proportional to to β (i.e., d/α) [19]. The presence of defects or the clamping effect can inhibit uniaxial domain (with d = 1) growth and can lead to domains with fractal dimensions, with "d" value less than 1 and corresponding β value less than 0.16. Our β values are very close to the theoretical value for a uniaxial ferroelectric with sharp square loop, indicating high quality films that is consistent with the SEM, RBS, and XRD results.

To confirm the dimension inferred from the exponent β in the I-O model and to explore the thickness dependence of domain width (the LLK law), we have analyzed in-plane PFM phase images of the BFO films. There have been several reports in the literature indicating that the film thickness has a direct influence on the domain size (width) [28,33,42]. The

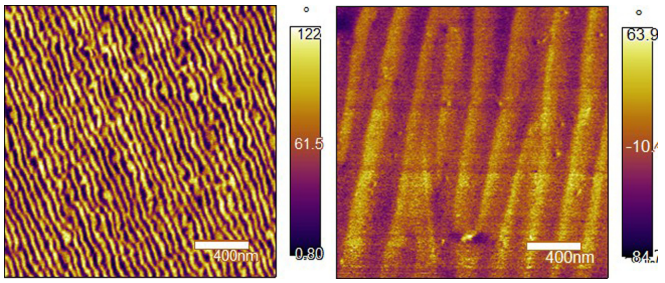

FIG. 7. In-plane phase images for different thickness BFO films [10 nm (left) and 110 nm (right)]. Both films show uniform striped domains. The domain wall density decreases whereas width of domains increases with thickness.

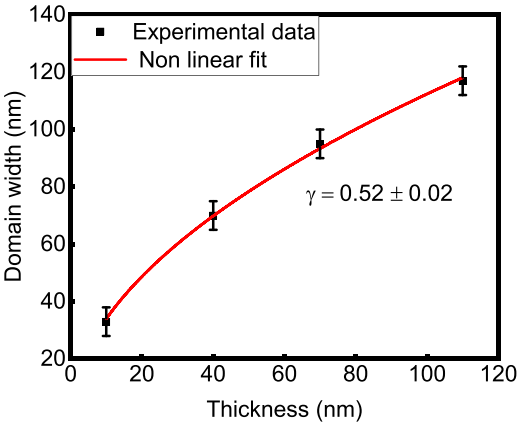

FIG. 8. Plot of domain width as a function of film thickness. The solid line is a power-law fit described by Kittel's law.

domain wall separates two opposite orientation regions of spontaneous polarization in a FE film. While uniform striped shape structures are observed for relatively thick BFO film ($\geqslant$100 nm) [42,43], thinner films display labyrinth-shaped complex and mixed contrast patterns [28,33,44]. The critical thickness for the change depends on the substrate, electrodes, and other growth process parameters [32]. Irregularly shaped domains for thinner films can be characterized by a fractal dimension. Due to the complex pattern, it is challenging to quantify their width using only PFM line scans [33,42]. It has recently been reported that post-annealing of the film facilitates formation of stripe domain pattern rather than fractal domains [45]. Indeed, we have observed stripe-like domains in our films over a wide thickness range after they are postannealed for one hour at the deposition conditions. Representative lateral PFM images for two different thickness films are shown in Fig. 7. Uniaxial striped domain patterns with uniform shape and sizes are observed for both films with "d" value near unity, consistent with the exponent obtained from power-law fit in Fig. 6. This provides direct confirmation of the dimensionality from PFM images. This uniformity in domain shape and sizes facilitates the fast switching, squared-shaped P-V loop with uniform coercive voltage for all the domains. It is clear from the images in Fig. 7 that the domain width varies with thickness, with the thinner film having smaller domains with higher domain wall density. The domain width for different thickness films has been quantified from the PFM line scans by tallying the number of domains across a defined straight segment. Figure 8 shows a plot of the estimated domain width as a function of film thickness. A power law fit yields an exponent of 0.52 $\pm$ 0.02, which is close to the Kittel law value of 0.5 considering the uncertainty. Some similar analyses reported in the literature have yielded exponents deviating from 0.5 [28,46]. This deviation may be related to the irregularity of the domain walls as observed in the PFM images. In pure FE materials (i.e., nonmultiferroic), domains are generally smaller than FM domains, however the FE domains of BFO are noticeably larger, which is consistent with the magneto-electric coupling observed in the material [28].

Since the domain shape and size evolve with film thickness, the coercive voltage and leakage current also vary with thickness as these parameters are intimately linked with the domain configuration. As the operating voltage of a FE device is usually larger than the coercive voltage, the thickness dependence of V_c is very important and it also provides valuable informations regarding the switching dynamics. We have investigated the thickness-dependent room temperature P-V loops of BFO at different applied frequencies. Representative P-V loops for different thickness films at 20 kHz are shown in Fig. 9. It is seen that while the polarization is virtually independent of film thickness, the V_c scales with thickness. The shape of hysteresis loops for 110–200 nm thickness films are nearly-square with essentially the same value of saturation (P_s) and remnant polarization (P_r). However, the P-V loop for the 70-nm film overestimates the polarization due to greater contribution from leakage current.

Due to the large leakage current contribution, it is difficult to obtain P-V loops at RT for even thinner films. Unsaturated P-V loops are obtained if very short pulses are applied with our electrode dimensions ($\sim$70 μm). The polarization values and coercive voltage obtained from such loops can be misleading. To circumvent this problem, PFM technique has been used to study the scaling behavior for thinner films since this technique is less sensitive to leakage current [31,44]. The corresponding switching voltage is determined from the phase loop obtained by using dual ac resonance tracking (DART) PFM. Figure 10 shows the plot of V_c vs thickness obtained

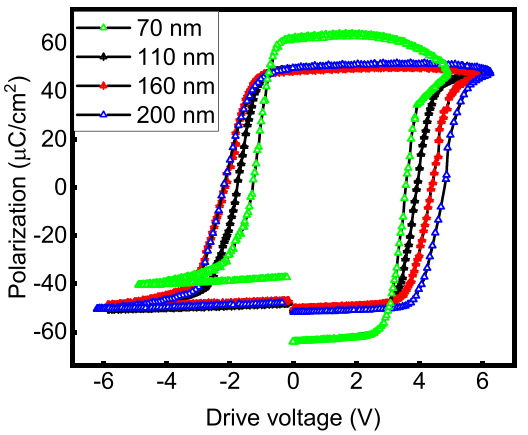

FIG. 9. P-V hysteresis loops measured at 20 kHz for BFO films with different thickness. These measurements are performed at room temperature.

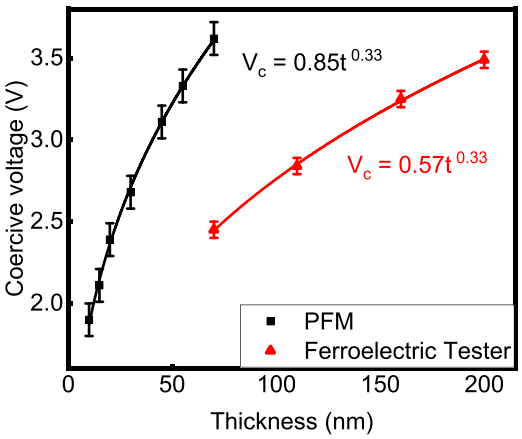

FIG. 10. Plot of V_c vs thickness for BFO films using two different techniques. The solid lines are nonlinear power-law fit to the observed data described by Kay-Dunn law. The scaling exponents for both fits yield 0.33. The black line corresponds to coercive voltages obtained from phase loop using PFM for relatively thinner films whereas the red one is for thicker films measured at 20 kHz using a ferroelectric tester.

both from ferroelectric P-V loops and PFM measurements for different thickness ranges. The exponents obtained from power law fits for both data sets are in agreement with the semi-empirical Kay-Dunn law. However, the coercive voltages obtained using PFM technique are systematically higher than those obtained from P-V hysteresis loops, which is consistent with previous reports [31,41,43,47]. This can be explained based on differences in the experimental measurement. The interfacial dead layer formed between the FE layer and the electrode junction plays an important role. In the PFM studies, voltage loss at the tip-sample interface can occur due to the thin layer of air between the tip and FE material, creating a parasitic capacitance. Also, the work function difference between cantilever tip and the sputtered Pt electrode can cause an offset in the switching voltage [31]. We could not grow films thicker than 200 nm due to experimental limitations. However, the Kay-Dunn law has previously been verified for BFO up to film thickness of $\sim$1 μm with measurements at 77 K [29].

For the thickness region in which P-V loops are not obtained due to high leakage current, the existence of nonvolatile memory of the films has been demonstrated using PFM lithography. This is a widely used technique to induce a local FE polarization reversal in a sample through the application of a bias voltage larger than the local switching voltage. The technique has been used to write a complex pattern by applying a dc bias through the conductive tip without altering the surface morphology [48]. The same tip is used to read the written polarization state after removal of the field. We have written a complex pattern on a 40-nm BFO film by applying $\pm$6 V dc bias. The retained phase (left) and amplitude (right) images upon removal of bias voltage is shown in Fig. 11. A clear contrast between up and down polarization states can be seen in the phase image indicating 180° phase switching.

The leakage current arising from electronic conduction under applied bias is a major drawback of BFO for device applications. Unlike other traditional FE materials, the relatively

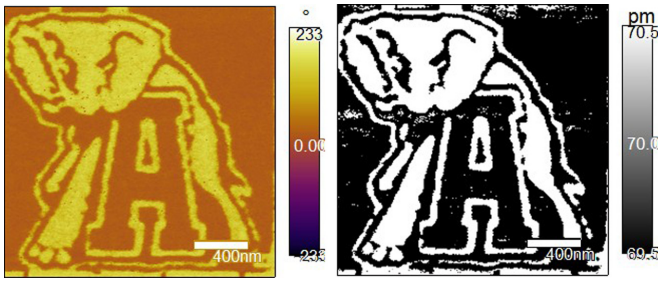

FIG. 11. PFM lithograph images of logo of The University of Alabama written on a 40-nm thick BFO film; phase image (left) and amplitude image (right) patterned in 2 μm$\times$2 μm area.

low band gap, propensity for defect formation and presence of partially filled d-orbitals are the primary sources of leakage current in BFO [7,43]. It is important to understand how the leakage current varies with film thickness since it determines the heating effect and hence the device performance. The leakage current mechanism in perovskite-based FE materials can be explained in two broad categories: FE material-electrode interface dominated mechanism and bulk-limited conduction mechanism. The Schottky emission arises from differences in Fermi levels between the metal electrode and FE film. Dominant FE material-electrode interface contribution results in the Fowler-Nordheim tunneling mechanism, which can contribute at high applied electric fields. On the other hand, Poole-Frenkel emission, arising due to consecutive hopping of charges between defect trap centers, and space-charge-limited current (SCLC) are bulk-limited conduction mechanisms [37,43,47]. Our measurement stack, i.e., Pt//BFO/SRO structure, can be regarded as a back-to-back connection of two Schottky diodes, due to the presence of Schottky potential barriers at each interface. In Pt//BFO//SRO capacitor structures, a mixed mechanism (combination of SCLC, Schottky, and Poole-Frenkel) has been reported [37,47].

We investigated the thickness-dependent leakage current over a wide range of applied voltage to determine the I-V characteristics. The corresponding I-V plots are shown in Fig. 12. Similar to the P-V loops, the leakage current plots are asymmetric due to the use of dissimilar electrodes. For

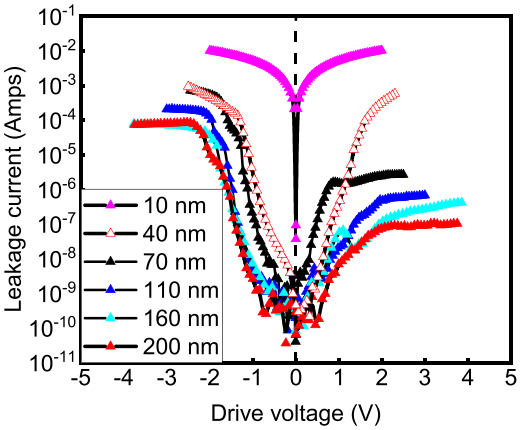

FIG. 12. Leakage current measured at room temperature for BFO films with different thickness.

films exhibiting closed P-V loops, the leakage currents are not significantly different. These results are consistent with the obtained saturated P-V loops and confirm that the measured polarization is intrinsic. However, for thinner films for which we are unable to obtain P-V loops, the leakage current is very high, with positive and negative branches of the leakage current being symmetric indicating the dominance of bulk-limited conduction mechanism and even shorting of the sample in extreme case. The decrease in leakage current with increasing film thickness is due to increase in grain size and decrease in domain wall density as the grain boundaries and domain walls are considered to be the primary conduction paths [24,30,49]. The increment in domain wall density for thinner film as seen in the lateral PFM images in Fig. 7 clearly supports this assumption. It has been reported that nonuniform polarization normal to the domain walls generates an electrostatic depolarizing field that may attract the charge carriers [32]. Moreover, for thicker films, the substrate clamping effect and effect of dead layer between electrode and film is reduced, which enhances the dielectric constant and ultimately reduces the leakage current [24,30].

IV. CONCLUSIONS

Various aspects of the switching dynamics and domain properties have been analyzed for high quality epitaxial BFO films as a function of film thickness and frequency of applied pulses. The dimensionality of domain walls obtained from PFM (static method) has been corroborated with that obtained from the I-O model (dynamic method). The domain width and coercive voltage scaling relationship have been studied using LLK law and Kay-Dunn law, respectively. With dominance of structural defects, such a close agreement with above-mentioned laws would have been unlikely. We also observe a clear qualitative correlation between domain wall density and leakage current. Our results clearly demonstrate the parametrization of the switching dynamics of BFO-based multiferroic material over a range of frequency and thickness of films. This study can also be helpful to understand functional relationship between domain properties and their effect on the switching characteristics in other ferroic systems.

ACKNOWLEDGMENTS

This work was supported by the Semiconductor Research Corporation (SRC) for a project in collaboration with Intel Corporation (SRC Contract No. 2018-IN-2833). The authors would like to thank Dr. Resul Yilgin for his involvement during the initial phase of work. We are grateful to Dr. Tanay Gosavi and Dr. Urusa Alaan for useful discussions and suggestions regarding the project. We also thank Rustem Ozgur at UC Berkeley for his suggestions and advice regarding the PFM measurements. We are thankful to Dr. Hussein Hijazi at Rutgers, The State University of New Jersey for RBS measurements.

[1] L. Martin, S. Crane, Y. Chu, M. Holcomb, M. Gajek, M. Huijben, C.-H. Yang, N. Balke, and R. Ramesh, J. Phys.: Condens. Matter **20**, 434220 (2008).
[2] W. Eerenstein, N. Mathur, and J. F. Scott, Nature (London) **442**, 759 (2006).
[3] R. Thomas, J. Scott, D. N. Bose, and R. S. Katiyar, J. Phys.: Condens. Matter **22**, 423201 (2010).
[4] S.-W. Cheong and M. Mostovoy, Nat. Mater. **6**, 13 (2007).
[5] J. Wang, J. Neaton, H. Zheng, V. Nagarajan, S. Ogale, B. Liu, D. Viehland, V. Vaithyanathan, D. Schlom, U. Waghmare *et al.*, Science **299**, 1719 (2003).
[6] R. Ramesh and N. A. Spaldin, Nat. Mater. **6**, 21 (2007).
[7] V. Shelke, D. Mazumdar, G. Srinivasan, A. Kumar, S. Jesse, S. Kalinin, A. Baddorf, and A. Gupta, Adv. Mater. **23**, 669 (2011).
[8] T. Zhao, A. Scholl, F. Zavaliche, K. Lee, M. Barry, A. Doran, M. Cruz, Y. Chu, C. Ederer, N. Spaldin *et al.*, Nat. Mater. **5**, 823 (2006).
[9] J. Allibe, S. Fusil, K. Bouzehouane, C. Daumont, D. Sando, E. Jacquet, C. Deranlot, M. Bibes, and A. Barthelemy, Nano Lett. **12**, 1141 (2012).
[10] S. Manipatruni, D. E. Nikonov, C.-C. Lin, T. A. Gosavi, H. Liu, B. Prasad, Y.-L. Huang, E. Bonturim, R. Ramesh, and I. A. Young, Nature (London) **565**, 35 (2019).
[11] Y. Chu, Q. Zhan, C.-H. Yang, M. Cruz, L. Martin, T. Zhao, P. Yu, R. Ramesh, P. Joseph, I. Lin *et al.*, Appl. Phys. Lett. **92**, 102909 (2008).
[12] H. Hojo, K. Oka, K. Shimizu, H. Yamamoto, R. Kawabe, and M. Azuma, Adv. Mater. **30**, 1705665 (2018).
[13] T. Moore and J. Bland, J. Phys.: Condens. Matter **16**, R1369 (2004).
[14] P. Barrozo, D. R. Småbråten, Y.-L. Tang, B. Prasad, S. Saremi, R. Ozgur, V. Thakare, R. A. Steinhardt, M. E. Holtz, V. A. Stoica *et al.*, Adv. Mater. **32**, 2000508 (2020).
[15] J. A. Ewing and H. G. Klaassen, Philos. Trans. R. Soc. London A **184**, 985 (1893).
[16] J. Smith and H. P. J. Wijn, *Ferrites–Physical Properties and Technical Applications* (Phillips Technical Library, Eindhoven, 1959).
[17] B. Raquet, R. Mamy, and J. C. Ousset, Phys. Rev. B **54**, 4128 (1996).
[18] H. Orihara, S. Hashimoto, and Y. Ishibashi, J. Phys. Soc. Jpn. **63**, 1031 (1994).
[19] Y. Ishibashi and H. Orihara, Integr. Ferroelectr. **9**, 57 (1995).
[20] S. Hashimoto, H. Orihara, and Y. Ishibashi, J. Phys. Soc. Jpn. **63**, 1601 (1994).
[21] S. M. Yang, J. Y. Jo, T. H. Kim, J.-G. Yoon, T. K. Song, H. N. Lee, Z. Marton, S. Park, Y. Jo, and T. W. Noh, Phys. Rev. B **82**, 174125 (2010).
[22] S. Singh, K. Maruyama, and H. Ishiwara, Integr. Ferroelectr. **98**, 83 (2008).
[23] A. Lahmar, J. Magn. Magn. Mater. **439**, 30 (2017).
[24] B. Yang, L. Jin, R. Wei, X. Tang, L. Hu, P. Tong, J. Yang, W. Song, J. Dai, X. Zhu *et al.*, Small **17**, 1903663 (2021).
[25] A. Ruff, Z. Li, A. Loidl, J. Schaab, M. Fiebig, A. Cano, Z. Yan, E. Bourret, J. Glaum, D. Meier *et al.*, Appl. Phys. Lett. **112**, 182908 (2018).

[26] Y. J. Shin, B. C. Jeon, S. M. Yang, I. Hwang, M. Cho, D. Sando, S. R. Lee, J.-G. Yoon, and T. Noh, Sci. Rep. **5**, 10485 (2015).
[27] J. Scott, Integr. Ferroelectr. **12**, 71 (1996).
[28] G. Catalan, H. Béa, S. Fusil, M. Bibes, P. Paruch, A. Barthélémy, and J. F. Scott, Phys. Rev. Lett. **100**, 027602 (2008).
[29] D. H. Kim, H. N. Lee, M. D. Biegalski, and H. M. Christen, Appl. Phys. Lett. **92**, 012911 (2008).
[30] S. Hussain, S. Hasanain, G. H. Jaffari, and S. I. Shah, Curr. Appl. Phys. **15**, 194 (2015).
[31] J. J. Steffes, R. A. Ristau, R. Ramesh, and B. D. Huey, Proc. Natl. Acad. Sci. USA **116**, 2413 (2019).
[32] G. Catalan and J. F. Scott, Adv. Mater. **21**, 2463 (2009).
[33] V. Shelke, D. Mazumdar, S. Jesse, S. Kalinin, A. Baddorf, and A. Gupta, New J. Phys. **14**, 053040 (2012).
[34] H. Kay and J. Dunn, Philos. Mag. **7**, 2027 (1962).
[35] M. Dawber, P. Chandra, P. Littlewood, and J. Scott, J. Phys.: Condens. Matter **15**, L393 (2003).
[36] R. Xu, R. Gao, S. E. Reyes-Lillo, S. Saremi, Y. Dong, H. Lu, Z. Chen, X. Lu, Y. Qi, S.-L. Hsu *et al.*, ACS Nano **12**, 4736 (2018).
[37] V. Shelke, V. Harshan, S. Kotru, and A. Gupta, J. Appl. Phys. **106**, 104114 (2009).
[38] M. Mayer, AIP Conf. Proc. **475**, 541 (1999).
[39] M. Bohra, K. Negi, V. Karthik, H. Chou, X. Wang, and W. Chu, Sci. Rep. **7**, 4501 (2017).
[40] A. Gupta, X. Li, and G. Xiao, J. Appl. Phys. **87**, 6073 (2000).
[41] E. Parsonnet, Y.-L. Huang, T. Gosavi, A. Qualls, D. Nikonov, C.-C. Lin, I. Young, J. Bokor, L. W. Martin, and R. Ramesh, Phys. Rev. Lett. **125**, 067601 (2020).
[42] Y. Chen, M. Katz, X. Pan, R. Das, D. Kim, S. Baek, and C. Eom, Appl. Phys. Lett. **90**, 072907 (2007).
[43] L. R. Dedon, S. Saremi, Z. Chen, A. R. Damodaran, B. A. Apgar, R. Gao, and L. W. Martin, Chem. Mater. **28**, 5952 (2016).
[44] Y. Chu, T. Zhao, M. Cruz, Q. Zhan, P. Yang, L. Martin, M. Huijben, C.-H. Yang, F. Zavaliche, H. Zheng *et al.*, Appl. Phys. Lett. **90**, 252906 (2007).
[45] Y. Nahas, S. Prokhorenko, J. Fischer, B. Xu, C. Carretero, S. Prosandeev, M. Bibes, S. Fusil, B. Dkhil, V. Garcia *et al.*, Nature (London) **577**, 47 (2020).
[46] W.-H. Kim and J. Yeog Son, Appl. Phys. Lett. **103**, 132907 (2013).
[47] G. W. Pabst, L. W. Martin, Y.-H. Chu, and R. Ramesh, Appl. Phys. Lett. **90**, 072902 (2007).
[48] For example, see https://afm.oxinst.com/assets/uploads/products/asylum/documents/Piezoresponse-Force-Microscopy-AFM-web.pdf.
[49] J. Seidel, L. W. Martin, Q. He, Q. Zhan, Y.-H. Chu, A. Rother, M. E. Hawkridge, P. Maksymovych, P. Yu, M. Gajek *et al.*, Nat. Mater. **8**, 229 (2009).